CHARACTERISTICS OF VARIOUS CONFINEMENT REGIMES OBTAINED WITH EC AND LH HEATING ON THE TdeV TOKAMAK

G.W. PACHER, R. DECOSTE, Y. DEMERS, J.-L. LACHAMBRE, F. MARTIN, C. COTE, J.-L. GAUVREAU, A. COTE, G. ABEL, R.A. BOLTON, C. BOUCHER, I. CONDREA, V. FUCHS, B.C. GREGORY, E. HADDAD, P. JACQUET, J. KALNAVARNS, D. LAFRANCE, G. LECLAIR, H.H. MAI, R. MARCHAND, F. MEO, D. PINSONNEAULT, B. QUIRION, N. RICHARD, A. SARKISSIAN, I.P. SHKAROFSKY, M.M. SHOUCRI, B. STANSFIELD, M. ST.-ONGE, and the TdeV TEAM
Centre canadien de fusion magnétique (CCFM),
Varennes, Québec, J3X 1S1
Canada

Abstract

Steady-state H-modes in type III ELM regime on TdeV with electron cyclotron and lower hybrid heating are investigated with respect to lower hybrid wave coupling, threshold power, helium pumping and separation between separatrix and surrounding structures. Energy confinement is found to improve as the distance between separatrix and divertor baffle is reduced. With off-axis EC heating, reduced particle transport is observed inside the deposition zone, but no energy transport barrier is obtained. New measurements on compact toroid fuelling are reported which indicate that further optimization of the injector is required.

1. INTRODUCTION:

TdeV (R~0.83m, a~0.22 m, κ~1.1, B=2 T, I<0.25 MA) is a divertor tokamak with biasable divertor plates and flexible plasma shape control to alter the divertor configuration. Additional heating power is provided by electron cyclotron resonance heating (ECRH, 110 GHz, up to 600 kW) and by lower hybrid current drive power (LHCD, 3.7 GHz, up to 1 MW). Well-controlled stationary H-modes have been obtained with both heating systems.

In the following section, lower hybrid wave coupling to the plasma in L- and H-mode are discussed, and the synergy between the two heating methods is examined. The third section describes the characteristics of the H-mode in TdeV. In the fourth section, the effect of on-axis and off-axis ECRH heating on the density profile is analyzed. The fifth section reports the observations on helium pumping in L and H mode, and describes the effect of divertor geometry. The sixth section provides an update on compact toroid injection experiments into TdeV.

2. LOWER HYBRID WAVE COUPLING AND SYNERGY WITH ECRH

Well-controlled H modes were produced with lower hybrid heating alone at an input power level of 350 to 450 kW (LH power 130-350 kW). At higher LH power levels, recycling and degassing increased, rendering the control of density difficult, so that H-modes were not stationary.

2.1. Antenna coupling in L and H-mode plasmas

In general, LH antenna coupling deteriorates when going from L to H-mode in similar plasma conditions. The reflection coefficient at the grill increases by up to a factor of two in H-mode plasmas because of the steepening of the density gradient near the separatrix and the resulting lower SOL density. Figure 1 displays edge density profiles in L and H-mode (averaged over ELM's) obtained from reflectometry. The change in reflection coefficient due to the H-mode depends on several factors: the distance d between the LH antenna and the separatrix, the direction of the ion ∇B drift, the ELM

frequency and amplitude, injected power, the launched $N_{||}$, etc. Figure 2 shows an example of the modulation induced by the ELM's on the reflection coefficient when antenna-separatrix separation *d* is 2.5 cm. The D_α emission, the antenna reflection coefficient, and the ion saturation current at the antenna are well correlated.

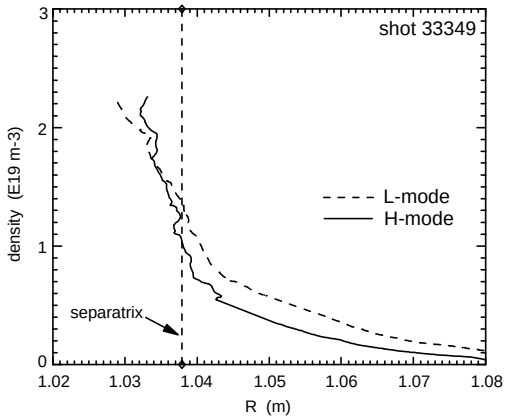

Fig. 1. Edge density profiles in L and H-mode

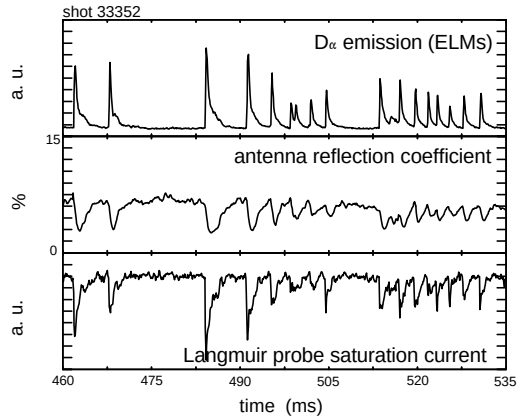

Fig.2. Effect of ELM's on antenna reflection coefficient in H-mode

In L-mode at high density, the total reflection coefficient rises to 10% as *d* is increased to 4 cm, but saturates at this value for distances as large as 10 cm. For *d*=10 cm, however, no H-modes were obtained, probably due to an influx of impurities at high LH power resulting from electrons accelerated at the antenna mouth and hitting machine structures not conceived to handle such a power flux. A moveable antenna guard limiter has been installed to mitigate this problem.

2.2. Current drive synergy between ECCD and LHCD in L-mode

To determine if the non-inductive current driven by a combination of LH+EC waves was higher than the sum of the currents driven by each system separately, a series of four shots was used, all with ~500 kW of EC heating (which essentially determines the temperature). It comprises EC heating alone, ECCD alone, EC heating with LHCD, and ECCD with LHCD. Comparison of the shots allows the different components of driven current to be deduced.

For EC deposition near *z*=0 cm, a synergy effect was observed with the combined systems driving ~8% (11.5 kA) more current than the sum of the currents for each system used separately in CD mode (115 kA of I_{LH} and 25 kA of I_{EC}). For deposition near *z*=5 cm (0.25 *a*), an anti-synergy effect was observed with the combined systems driving ~10% (16 kA) less current than the sum of the currents for the RF systems used separately (118 kA of I_{LH} and 40 kA of I_{EC}). Besides the deposition radius, the only difference between these cases was $\bar{n}_e$ = 1.8x10^{19} m^{-3} in the first case and $\bar{n}_e$ = 1.2x10^{19} m^{-3} in the second case. More experiments are planned to investigate these effects.

Simulations have shown that good synergy should be obtained when combining LH and EC waves in certain regions of physical and parameter space [1]. More simulations involving the whole plasma volume are however needed for direct comparison with experiments.

3. CHARACTERISTICS OF THE H-MODE IN TdeV

Well-controlled stationary H-modes have been obtained with both ECRH and LHCD heating systems. With the additional power applied (<500 kW), these H-modes remain in the type III ELM regime [2]. Power thresholds are comparable with those predicted by the ITER scaling laws. A pronounced threshold in edge density is observed, below which no L-H transitions occur. Line-average densities were limited to below ~6x10^{19}m^{-3} because at higher densities, ECRH is limited by refraction and cut-off and LHCD by accessibility. The plasma density is controlled by gas fuelling,

mainly in the plasma chamber, and by divertor pumping (~5 m^3/s). The density profile is modified by the additional heating power. Steady-state H-modes (which require control of edge density – see below) are thus obtained by using as a control signal one channel of the interferometer, whose impact parameter is ~0.6 of the plasma minor radius.

An extremely strong dependence of the H-mode transition on the separatrix density was observed. When the density was not well-controlled, repetitive L-H transitions were observed which occurred at precisely the same value of separatrix density, 1.5x10^{19} m^{-3}. The back transitions were all obtained at a lower value, 1.3x10^{19} m^{-3}. When the separatrix density was held constant above the H-L threshold steady-state H-modes were obtained for the duration of the heating power pulse. For such shots, an increase of the type III ELM frequency with decreasing separatrix density is clearly observed, indicating that the power threshold is approached as the density decreases.

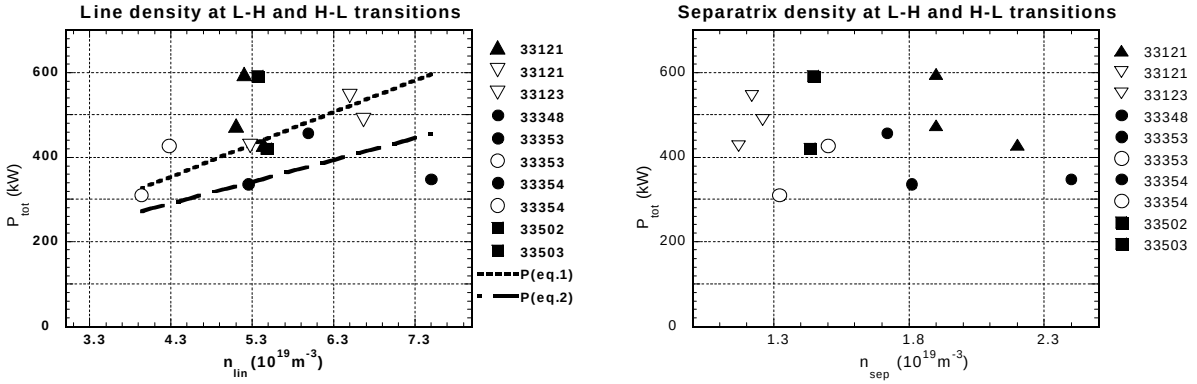

Fig. 3. Total input power vs. line average density at the L-H threshold. Filled symbols denote L-H transitions, open symbols H-L transitions. Ohmic-heated values are indicated by open circles, lower-hybrid heating by filled circles. All values except for the two filled squares are for ÑB drift towards the divertor. The ITER threshold power scaling laws are indicated for reference by thick lines, dotted without and dashed with elongation dependence.

On Fig. 3, the input heating power at the transition has been plotted against line average and separatrix density respectively. These plots include both L-H transitions for ECRH with favorable ∇B drift, ECRH with unfavorable ∇B drift, and Lower Hybrid heating with favorable ∇B drift. For the H-L back transition, only points for ECRH with favorable ∇B drift and OH alone after ECRH turn-off are plotted. In terms of the line-average density, the lower values of threshold power are consistent with the ITER H-mode power threshold scaling laws [3]. No significant hysteresis is obtained between L-H and H-L transitions, nor is there a significantly different power threshold for the two ∇B directions. In terms of the separatrix density, there is a clear separation between the L-H and the H-L threshold, as expected from the discussion in the preceding paragraph. The L-H transition for the "unfavorable" ∇B direction actually lies at lower values of separatrix density, comparable to those for the H-L transition with "favorable" ∇B .

3.1. Variation of gaps

H-modes were obtained as distance between separatrix and the divertor baffle was reduced to less than one density scrape-off layer in L-mode ($\Delta_{L\text{-}SOL}$~15 mm at the midplane, ~10% of flux). The time to H-mode transition increases somewhat, from ~15 to ~19 ms, and is accompanied by a slight increase in ELM repetition rate. Only at the smallest distance of 0.7 $\Delta_{L\text{-}SOL}$ was there an appreciable increase both in time to transition (50 ms for this shot series) and in ELM frequency (~x2) [4]. These effects indicate that the power threshold increases as the separation is reduced. Similar conclusions can be drawn from the effect of reducing the distance between separatrix and outboard limiter to less than one $\Delta_{L\text{-}SOL}$.

3.2. H-mode confinement with reduced gaps

On Fig. 4, the ratio of stored energy from diamagnetic measurements in H-mode to that in L-mode is plotted for the gap variations and for the same shot series described above. As the outboard separation is reduced, the confinement appears to degrade. However, an improvement in H-mode confinement over L-mode is observed as the separatrix to divertor baffle distance is reduced (as discussed above, the smallest separation had a much higher He content, and is therefore only joined with a dashed line). This experiment was repeated for gaps of 2.5 and 0.7 $\Delta_{L\text{-}SOL}$ and now confirms that at similar helium contents, the ELM amplitude is decreased, the ELM frequency is increased, and the confinement is improved for the smaller separatrix-divertor baffle gap (Fig. 4 – filled diamonds – we compare only the trend, and not the absolute values because the machine conditions were probably quite different). However, the sharp increase in confinement at small baffle separation was not seen for these conditions.

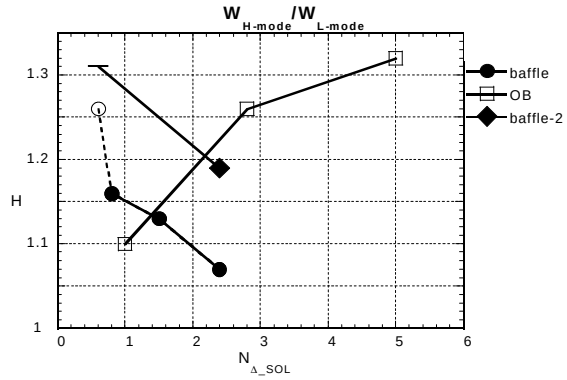

Fig. 4. Ratio of diamagnetic measurement in H-mode to that in L-mode plotted against gap width expressed in number of L-mode density scrape-off layers. Round symbols for separatrix. divertor baffle gap (results for same He concentration are filled diamonds), square for decreasing outboard separatrix. limiter gap.

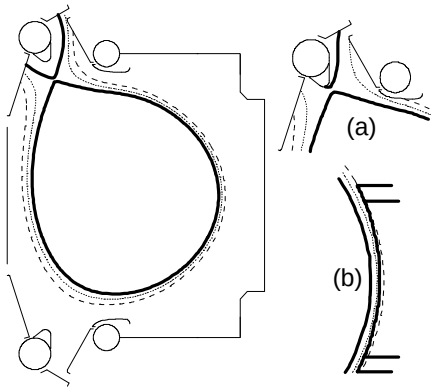

Fig. 5. Illustration of the magnetic geometry of TdeV indicating minimum gaps for figure 4. Flux is plotted as 5% contours

3.3. Effect of biasing on the H-mode

Divertor plate biasing [5] mainly influences the edge of the discharge and can therefore control H/L mode transitions. Negative (positive) biasing is detrimental (favorable) to the H-mode as shown on Fig. 6.

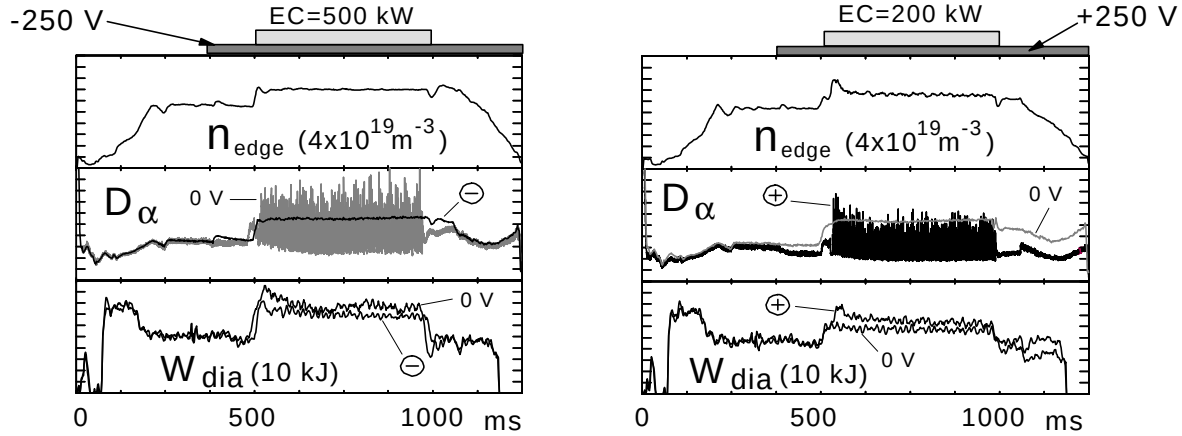

Fig. 6. Effect of negative (left) and positive (right) biasing on the H-mode

With 500 kW of ECRH and no biasing, a stationary H-mode is obtained. When -250 V is applied to the divertor plate with respect to the vessel, the discharge turns into L-mode at the same edge density. When the discharge is operated just below the threshold with 200 kW of ECRH and no

biasing, applying +250 V induces a stationary H-mode during the whole EC period. Reversing the toroidal field and plasma current polarity (anti-parallel in TdeV), does not reverse this effect; negative biasing remains detrimental to H-mode and positive biasing favors it regardless of B_T direction. Our results on biasing polarity, contrary to those of JFT-2M [6], confirm the theory that H/L transitions are governed by the radial electric field gradients and not its polarity.

4. PROFILE MODIFICATIONS IN H-MODE WITH ON AND OFF-AXIS HEATING

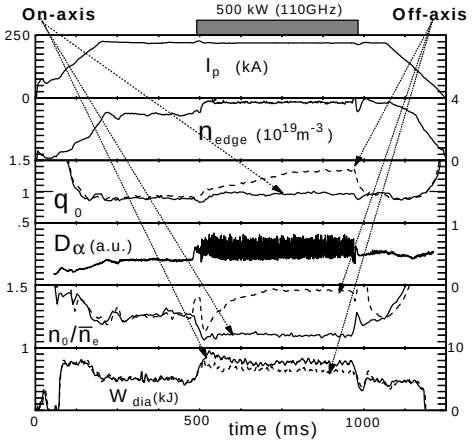

Fig.7. Time development of parameters during on and off-axis heating in H-mode

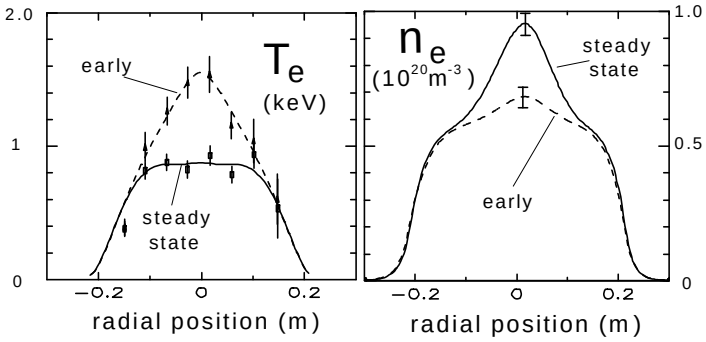

Fig. 8. Early (dashed) and late (full) profiles during off-axis heating in H-mode

Figure 7 compares stationary H-modes obtained with central and off-axis (r/a=.65) EC heating. The peaking factor curves, $n_0/\bar{n}_e$, demonstrate that central power deposition flattens the density profile whereas during off-axis deposition the initially flat profile peaks progressively. The temperature profiles exhibit a complementary behaviour (Fig. 8) such that the local pressure is approximately constant, as is the diamagnetic energy. The central safety factor q_0, is close to unity during on-axis deposition and evolves from 0.9 to 1.3 during off-axis heating, consistent with neoclassical resistivity. The evolution of the density profile for the off-axis case over a characteristic resistive time suggests that the current penetration is important for density peaking. Density peaking is also observed in L-mode with off-axis heating at high densities but disappears completely below $\bar{n}_e \approx 3\text{x}10^{19}\text{m}^{-3}$.

Figure 9 presents the incremental particle diffusion coefficient and pinch velocity (deduced from gas modulation experiments) for the early (flat density profile in Fig. 8) and late phase (peaked profile of Fig. 8) of the EC heating period. Consistent with the observed temporal penetration, both coefficients are significantly larger for flat $n_e(r)$ than for peaked $n_e(r)$, indicating a transport barrier near the deposition radius for the peaked profile. An ASTRA [7] heat transport analysis of these two cases has been performed. The experimental T_e and n_e profiles and experimental diffusion coefficients and particle pinch are inputs to the analysis. Neoclassical ion energy transport is assumed, with a factor adjusted to fit the measured axial values. As seen on other machines (DIII-D, RTP), a negative electron heat flux inside the deposition radius is deduced opposing the temperature gradient in both cases. Accordingly, non-diffusive heat transport such as non local transport or a heat pinch which could result from suprathermals or trapped electrons must be invoked. Heat flux is reduced inside the confinement zone with respect to on-axis heating. Contrary to particle transport, the energy flux does not, however, change with the density profile.

5. HELIUM EXHAUST

Pumping is performed in the active divertor only via the slot between the near-horizontal and near-vertical divertor plates (Fig. 10), using a commercial cryosorption pump efficient for both deuterium and helium. Helium is puffed in the main chamber early in the discharge and its decay time

constant (t^*_p) is measured in the main plasma. Using a two-reservoir model, t^*_p is related to He compression (C_{He}) from which the enrichment (h) is calculated [8]. Figure 10 shows the divertor pressure, He partial pressure and enrichment obtained with and without EC heating with outboard (OB) and private region (PR) pumping geometries. OH results are also shown. H-modes appear to have only a small effect on divertor pressures. The increased particle confinement obtained from the edge barrier is cancelled by the loss of confinement effect due to strong heating, however the He enrichment is seen to decrease by about 25%. On the other hand, the L-mode doubled the divertor pressures with respect to ohmic discharges and provided a 25% increase in enrichment. For both ohmic and H-mode, better He exhaust is obtained for outboard (OB) than for private region (PR) pumping.

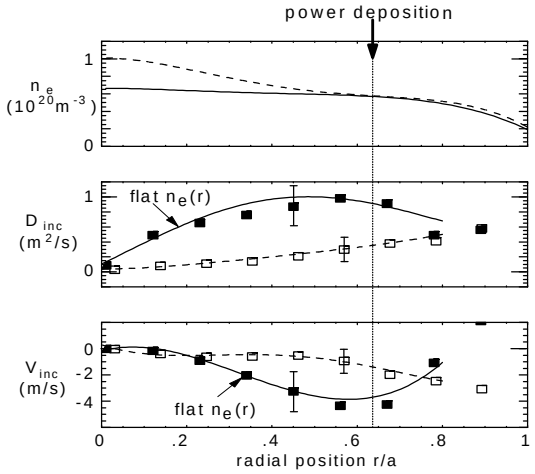

Fig. 9. Particle transport coefficients deduced from gas modulation experiments for flat and peaked H-mode profiles

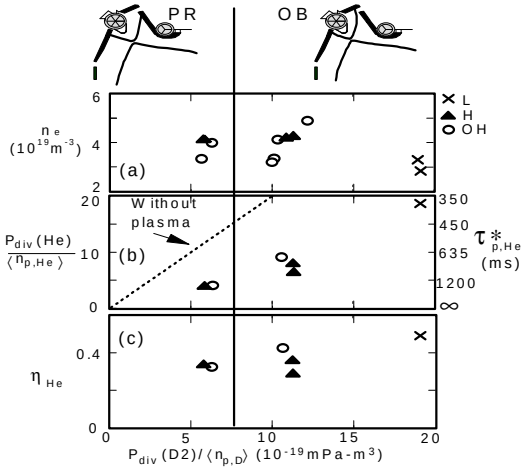

Fig. 10. Helium exhaust for OH, H and L-modes. Plasma density(a), divertor helium pressure and helium global confinement time (b), and helium enrichment (c) against divertor deuterium pressure.

6. INJECTION OF COMPACT TOROIDS (CT)

Compact toroids (CT) have been injected into the tokamak plasma of TdeV. An off axis (r/a $\approx$0.5-0.6) increase of the electron density on a fast time scale (~ 0.5 ms) was observed and has been interpreted as an indication of direct CT fuelling of the tokamak plasma [9]. More recent faster time scale (10μsec) measurements the CT visible bremsstrahlung emission and of the line integrated electron density have been performed, for injection both into a toroidal field (without tokamak plasma) and into a tokamak plasma are reported here.

For injection into a toroidal field, the visible bremsstrahlung measurements (fig. 11a) indicate CT penetration of the magnetic field on a fast time scale (~ 20μsec). Part of the plasma expands along the toroidal field lines and is observed on the same time scale by the interferometer situated in the diagnostic port adjacent to that of CT injection (l $\approx$34. cm). A significant portion of the injected plasma is subsequently ejected from the higher toroidal field region by the J $\times$ B force associated with the ∇B drift on a time scale of 50-60 μsec consistent with the outward acceleration ($dv/dt \sim 2\, c_s^2/R$, $T_e \sim 5$ eV) predicted by theoretical modeling [10]. The density deposition profile as observed by the interferometry measurements increases radially outward. CT penetration for injection into a toroidal field is qualitatively consistent with the CT penetration model [11].

For CT injection into a tokamak plasma, the visible bremsstrahlung chords outside the separatrix register a prompt (~20μsec) signal of the same level as for injection into a toroidal field of equal value but the chords passing inside the separatrix show a much weaker prompt signal. The line integrated density (plasma chords) increases on a slower time scale (~200μsec). A time/radial position

contour plot of the line integrated density increment (fig. 11b) shows the density increase moving inward from the edge of the tokamak plasma (separatrix), producing an axi-symmetric density increase at r/a ≈0.5-0.6 in about 1.0 msec. The estimated diffusion coefficient associated with this inward transport of plasma (D ~ 10 m^2/sec) is much greater than normal published values.

Bremsstrahlung measurements indicate a prompt (~ 20μsec) rise only on chords outside the separatrix in the presence of tokamak plasma, whereas all chords rise rapidly when only the toroidal field is present. Similarly, interferometry exhibits a fast rise on a similar time scale for the latter experiment, and a slower increase (~200μsec) during a tokamak discharge. A time/radial position contour plot (Fig. 11) of the line integrated density increment clearly shows the density increase coming from the edge of the tokamak plasma (separatrix) moving inward before peaking.

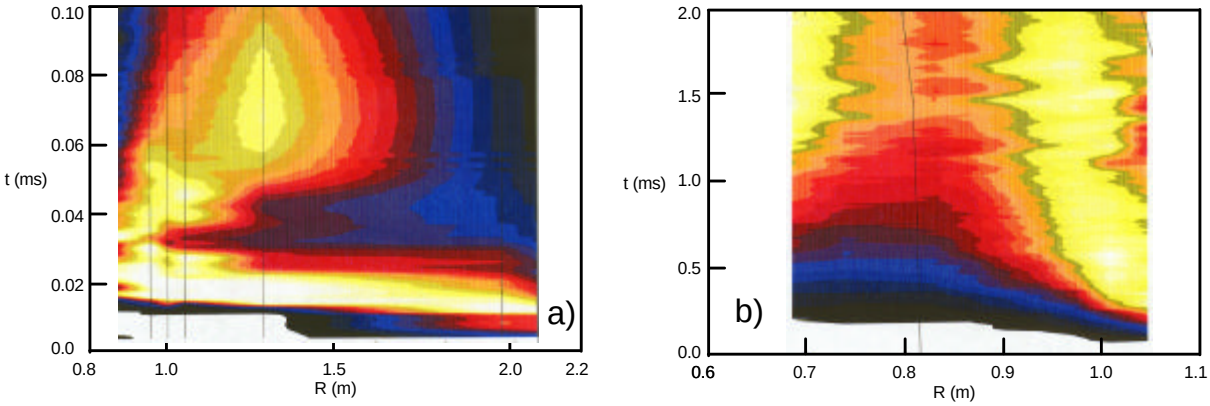

Fig. 11. False color contour plots of (a)visible bremsstrahlung emission from CT plasma injected only into a toroidal field (0.4 T) and (b) interferometer signal increment on injection into a tokamak plasma at 1.07 T. The ordinate represents time, the abscissa major radius, (plasma center at 0.83 m, plasma edge at 1.08 m). Bright colors denote high density. Note the different time scales

The tokamak plasma thus significantly modifies the progression of the injected plasma. A possible explanation is that, for the CT's produced for the TdeV injection experiments, only a small portion of the injected plasma was included in the CT magnetic fields, the major part trailing behind the spheromak with a velocity close to the CT velocity (e.g. trailing plasma produced by the CT gun [9] or plasma shed by the CT spheromak). This non spheromak plasma can transverse a magnetic field because of the drift associated with the self-consistent Hall electric field. However, this plasma will not penetrate significantly past the separatrix because the finite perpendicular conductivity of the tokamak plasma short circuits the Hall electric field. It is hypothesized that this plasma component effectively fuelled the tokamak plasma (from the edge) in the TdeV experiments.

CT fuelling of a tokamak plasma thus requires an optimization of the CT injector so as to maximize the plasma confined in the spheromak which can then penetrate the tokamak plasma (not just magnetic field) and deposit its fuel.

7. CONCLUSION

Steady-state H-modes in type III ELM regime have been produced on TdeV with electron cyclotron and lower hybrid heating. LH wave coupling becomes more difficult in H-mode because of the steeper edge density gradient. In L-mode, a small degree of synergy between the two current drive systems has been demonstrated. Further theoretical and experimental work is required to optimize this effect.

The input power for L-H transition is consistent with the ITER threshold power scaling laws. In terms of line-average density, no hysteresis is observed between L-H and H-L transitions. The L-H transition in TdeV is extremely sensitive to the separatrix density, which manifests itself as a threshold

density below which no L-H transitions were obtained with the available power. In terms of separatrix density, there is a clear hysteresis between L-H transitions, which occur at a higher value than H-L transitions for the same input power. Positive biasing of the divertor plate with respect to the vacuum vessel reduces the H-mode power threshold at the same edge density, whereas negative biasing increases it.

H-modes were obtained with an outboard separatrix-limiter distance less than or of the order of one density scrape-off length. The confinement at the smallest distance was reduced by about 10%. Reduction of the separatrix-divertor baffle distance in a similar fashion improved the H-mode confinement over a more open configuration.

Off-axis EC heating manifests itself in gradual peaking of the density profile on a resistive time scale and gradually reduced particle transport region inside the deposition zone. No change in energy flux is observed. However, only a non-diffusive energy transport inside the deposition radius is consistent with the observed pressure profiles.

Helium exhaust in H-mode is reduced by ~25% with respect to ohmic heated plasmas, and by ~50% with respect to L-mode plasmas. The total divertor pressures were comparable for the three cases. For both ohmic and H-mode, better He exhaust is obtained for outboard (OB) than for private region (PR) pumping.

Fast time-scale measurements indicate that only a small fraction of the plasma injected by the CT fueller penetrated well past the separatrix into the tokamak plasma, whereas the totality penetrated a purely toroidal field. An hypothesis has been exposed which explains the observations, and indicates that further optimization of the CT injector to maximize the quantity of plasma magnetically confined in the spheromak is necessary to assure more central CT fuelling.

Acknowledgements

CCFM is supported by the Government of Canada, Hydro-Québec, and INRS. The authors gratefully acknowledge the support of the Max Planck Institute für Plasmaphysik (Garching) and the Kurchatov Institute for providing the ASTRA code package and thank G.V. Pereverzev for his help in its use.

References

[1] M. Shoucri, *et al*, Proc. 25th EPS Conf. On Controlled Fusion & Plasma Physics, Prague (1998).
[2] Zohm, H. Plasma Phys. Contr. Fusion 38 (1996) p.105.
[3] The ITER H-mode Threshold Database Working Group (pres. by Snipes, J.A.), in Controlled Fusion and Plasma Physics (Proc. 24th Eur. Conf. Berchtesgaden, 1997), Part III, European Physical Society (1997) p. 961
[4] G.W. Pacher, *et al*, 13th PSI Conference, San Diego (1998), to be publ. in J. Nucl. Mat.
[5] J.-L. Lachambre, *et al.*. Nucl. Fusion, **34**, 1994
[6] T. Shoji et al., Proc. 14th Conference on Plasma Phys. Control. Fusion, Wuerzburg (1992), vol. 1, 323
[7] G.V. Pereverzev, *et al.*, IPP Report No. 5/42
[8] J.-L. Gauvreau, *et al*, 13th PSI Conference, San Diego (1998), to be publ. in J. Nucl. Mat.
[9] R. Raman, *et al.*, PRL 73, 3101 (1994); R. Raman et al., Nuclear Fusion 37, 967 (1997), R. Raman, *et al.*, Proc. 24rd EPS Conf. On Controlled Fusion & Plasma Physics, Berchtesgaden (1997)
[10] L.L. Lengyel, Nuclear Fusion 17, 805 (1977), V. Rozhansky et al., Plasma Phys. Control. Fusion 37, 399 (1995)
[11] L.J. Perkins et al., Nuclear Fusion 28, 1365 (1988)